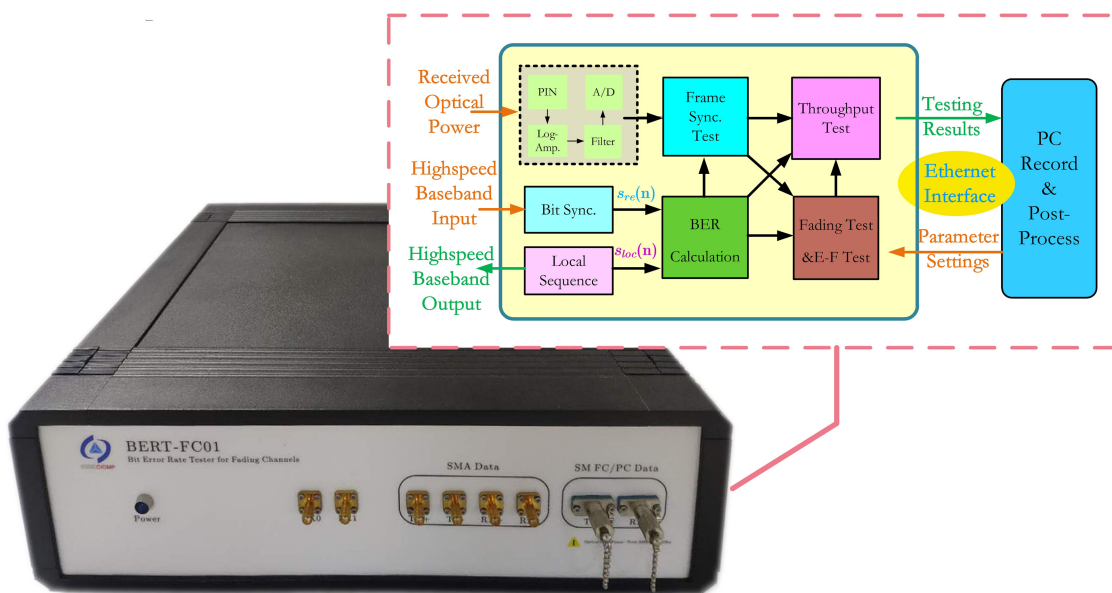


Measurement Approaches and Implementation of a Fading Characterization Tester for Evaluating Optical Turbulent Channels


Volume 12, Number 6, December 2020

Yatian Li, *Member, IEEE*
Tianwen Geng
Xueliang Li
Ye Wang
Shijie Gao



DOI: 10.1109/JPHOT.2020.3036413

Measurement Approaches and Implementation of a Fading Characterization Tester for Evaluating Optical Turbulent Channels

Yatian Li ¹, *Member, IEEE*, Tianwen Geng,¹ Xueliang Li,¹
Ye Wang ^{1,2} and Shijie Gao¹

¹Changchun Institute of Optics, Fine Mechanics and Physics, Chinese Academy of Sciences, Changchun 130033, China

²University of Chinese Academy of Sciences, Beijing 100049, China

DOI:10.1109/JPHOT.2020.3036413

This work is licensed under a Creative Commons Attribution-NonCommercial-NoDerivatives 4.0 License. For more information, see <https://creativecommons.org/licenses/by-nc-nd/4.0/>

Manuscript received March 1, 2020; revised October 26, 2020; accepted November 3, 2020. Date of publication November 6, 2020; date of current version December 4, 2020. This work was supported in part by the National Natural Science Foundation of China under Grant 51605465, and in part by the Research Project of Scientific Research Equipment of Chinese Academy of Sciences. Corresponding author: Yatian Li (e-mail: yt_li@ciomp.ac.cn).

Abstract: Optical wireless communication (OWC) systems can exhibit high percentage availability, yet suffering from frequent intensity fades caused by turbulence effects and pointing errors. The intuitive method to character the link is using commercial bit error rate testers (BERT) by measuring the output sequence of the receiver, which provides limited information. Thus we propose the algorithms for measuring the outage and synchronization performance, bit error rate (BER), throughput, and fading statistics. The inputs consist of decoded data sequence and received optical power. Both the bit level and packet level measurements are presented. Then a fading characterization tester (FCT) having these functions is implemented based on a field programmable gate array (FPGA). Our indoor experiment reveals the measurement accuracy of the FCT by comparing the measured results with the derived theoretical ones. Another 1.9 km OWC experiment is also carried out. These measured results by FCT are presented, which can not only measure the OWC link, but also help the researchers to improve the system performance, such as the design of error correction approaches like forward error correction, the design of packet based network protocols.

Index Terms: Free space communication.

1. Introduction

Optical wireless communication systems are rapidly developed, because its tremendous bandwidth, security, license-free operation, etc [1]–[3]. The intensity modulation and direct detection (IM/DD) system has more simplicity to implement, while the coherent modulation has the ability of achieving higher data rates [4]–[7]. NASA's Lunar Laser Communication Demonstration (LLCD) mission has made a great success in 2013, where the optical link was achieved between the lunar orbiter and its ground segment (LLGT) with the data rate of 622Mbps [8]. Future plans for the next generation earth relay optical communications have been designed, where the space to ground links from optical relay satellites will have the ability of processing data with the rate of 100Gbps [9].

Despite the bright future, there are also some inevitable challenges hampering the system performance when transmitting through the atmosphere. Due to the eddies with different sizes, the turbulence channel would lead to intensity's scintillation and phase's perturbation in the receiving end [10]. The optical link also suffers from the inter-symbol interference (ISI). The optical path differences resulting from fractions can bring about different timing delays at the receiving lens, which causes ISI [11], [12]. The ISI also leads from synchronization errors, which always occur in the OWC links with high mobility [13]. Besides, additional outage events can be incited by pointing errors [14], [15].

When evaluating the link, researchers always use BER as the common evaluation index. To be employed in the practical systems, some FPGA-based BERTs have been designed. Y. Fan proposed a scheme for BER testing by FPGA that consisted of a BER tester (BERT) core and an additive white Gaussian noise (AWGN) generator core [16]. In Ref. [17], a BERT with fiber interfaces was depicted. In a point-to-point serial optical link setup, BER versus receiver sensitivity of an optical link was measured. A quasi-analytical method was proposed to estimate the BER for the complex communication system, based on the Best Linear Approximation (BLA) model to determine the signal-to-distortion ratio [18]. Ref. [19] has proposed an optimal logarithmically-symmetric confidence interval estimator for the ratio of BER estimates derived from two negative binomial tests. Negative binomial sampling can be recommended for comparison experiments where BER is the key metric. However, the performance of traditional BERT is not as good as the AWGN channels for OWC systems, due to the frequent fades are caused by these factors illustrated above. For example, let's consider a single 3 ms fade event occurs during the test period. We assume that a packet is considered lost if arbitrary errors happen in this packet. Considering a case that the packet length is 1 us, only 3000 packets are lost. During the measurement of 1 s, the packet throughput is 99.9995%. If the 3 ms fade is dispersed into several 0.03us fades uniformly across each 1us packet, the throughput turns to 99.83%. However, the two cases have the same BER results, while their throughputs are not the same. Besides, the BER results vary versus different measurement periods, but the fading events are unchanged. For example, the BER is equal to 3×10^{-3} over 1 second, and turns to 5×10^{-5} over 1 minute. That is to say, conventional BERT does not have the ability to character the fading channel. To the best of the authors knowledge, only a few literatures developed the special BERTs for the optical fading channel [20], [21], whose architectures were both based on FPGA. Ref. [20] proposed a device able to measure BER distribution, it can help to design efficient error correction scheme for optical links. In Ref. [21], a custom BERT has been designed that can disambiguate the effects of fade induced errors on channel throughput, where real time bit-level analysis of BER was also evaluated. BER was chosen as the threshold to determine synchronization status. It can be considered as the optimal threshold in the scheme of ISI-free system. But it's not the case when the ISI introduces an inevitable degradation.

Motivated by these literatures, the main purpose of paper is to present an approach to evaluate the optical fading channel objectively and comprehensively with the name of FCT, which can be implemented by FPGA fabric. The FCT can be either integrated in digital receiver or performance as a stand-alone test instrument. Different from current literatures, it has the ability of evaluating the outage and synchronization performance, BER and its distribution statistics, throughputs of the bit level and packet level, the error-free histograms and fading histograms. The main contributions of the FCT are listed here. First, the FCT conceives of both BER and the received power as the threshold of the outage declaration. In this way, the hamper of ISI can be intuitively measures. With the results of BER and throughput, the maximum effective information transmission rate of the link can be measured then. Moreover, the optimal packet length can be determined, according to the error-free and fading histograms and packet level throughput. Besides, forward error correction (FEC), automatic repeat-request (ARQ), or other diversity techniques can be optimized or designed according to the results of BER distribution and fading histograms. In addition, this paper derives the theoretical expressions of outage probability, BER and its distribution, mean fading time, which conform the indoor experimental results. Another field trial with the distance of 1.9 km has been carried out. The first measurement results are presented. It needs to be mentioned that some

TABLE 1
Main Variables and Their Brief Definitions

Name	Paraphrase	Name	Paraphrase
$B_{syn}^{(i)}$	bit level sync status for the i -th group	N_{out}^b, N_{out}^f	outage counters in bit or packet level
$F_{e-f}^{(i)}, F_{syn}^{(i)}$	error free or sync status for the i -th packet	$P_e^{(k,N)}$	BER for the i -th group with N bits
$f_h(h), f_{P_e}(P_e)$	PDF of channel gain h or BER P_e	$P_{e,th}$	threshold for outage determined by BER
$f_{h,h'}(h, h')$	joint PDF of h and its time derivative	$P_{e,isi}, P_{e,tsi}$	BER with or without ISI
$H_{e-f}^{t_{e-f}}$	error-free histograms for t_{e-f}	P_{out}^b, P_{out}^f	outage probability when $I < I_{th}$ or $P_e > P_{e,th}, I > I_{th}$
$H_{fad}^{t_{fad}}$	fading histograms for t_{fad}	P_{out}	total outage probability
I_{th}	power threshold for outage events	P_t	transmitting power
l_{e-f}, l_{fad}	number of groups for time t_{e-f} or t_{fad}	T_{fad}^{mean}	mean fading time
N_{e-f}, N_{fad}	counter of error-free or fading packets	t_{fad}^i, t_{e-f}^i	unit for error-free or fading measurement
$N_{e-f,th}$	threshold of error-free bits for sync state	$\Theta_b^{(i)}, \Theta_{pac}^{(i)}$	throughput for bit or packet level

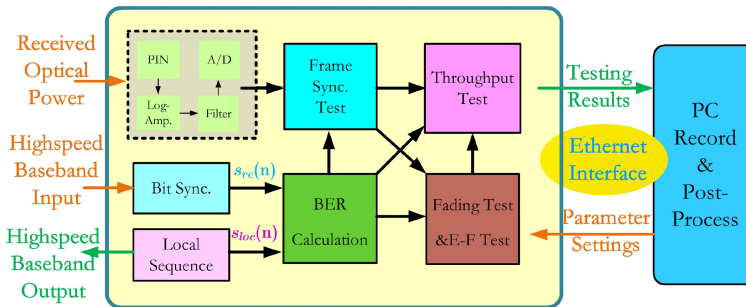


Fig. 1. The structure diagram of FCT.

theoretical expressions are derived that describe the outage performance, BER and its distribution and mean fading time.

The remainder of this paper is organized as follows. We depict the structure of the FCT in Section 2, as well as corresponding algorithms given in pseudo code diagrams. In Section 3, some theoretical expressions are derived, where the expressions in Sections 3.1–3.3 are corresponding to the parameters measured by FCT in Section 2.1–2.3 respectively. The indoor experiment and corresponding results are described in Section 4.1, while the field trial is illustrated in Section 4.2. In the end, conclusions are drawn in Section 5. For brevity, the variables used in this article are summarized in the Table 1. Note that the superscripts \bullet^{theo} denote the theoretical results of the variable \bullet , while the superscripts \bullet^{ms} represent the measured results of the variable \bullet . The \bullet_{th} in the subscript represents the threshold. The integer $\bullet^{(i)}$ in the superscript stands for the measured result for the i -th group. Besides, the super scripts \bullet^{se} mean the parameters set by the users.

2. System Structure & FCT

The purpose of designing the FCT is to measure the optical communication link quantitatively and accurately. The structure of the FCT is given in Fig. 1. As a whole, the FCT has two main input interfaces, which are the optical signal input and the high-speed baseband input, respectively. The former is responsible for counting the power characteristics of the received optical signal. It may connect a fiber coupler, which splits a little energy from the received optical signal. In this way, a negligible loss can be made on the photoelectric conversion progress for the receiver. The high-speed baseband input is responsible for evaluating the features of the OWC link. It should connect to the output of optical receivers, where the decoded data are transmitted serially. In the sequel, the FCT can be utilized in the cases of different modulation formats.

To implement the FCT in the FPGA, the utilized FPGA needs to have the ability of processing high speed baseband signals. We choose the FPGA from Xilinx 7 series Family. As depicted in Fig. 1, the left part is the FPGA-based main body, while the right part is the host PC calculating the results

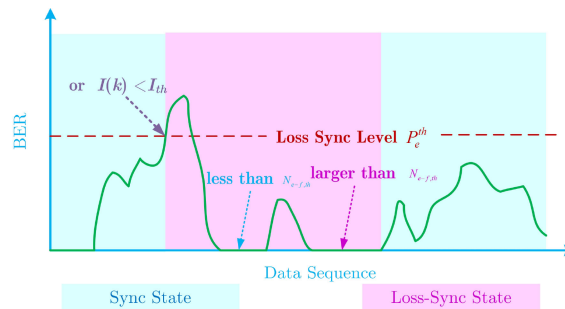


Fig. 2. The sync-in and outage judgment mechanism.

transmitted from the left part through an Ethernet link. The directed arrows denote the information transmission. The parameters in the main body can also be set up through this link. As mentioned in Section 1, the FCT has four critical functions, which are calculating the BER, evaluating the throughput, analyzing the outage and synchronization performance and computing the fading statistics, respectively. The corresponding modules are the green part (BER Calculation Module, BCM), purple part (Throughput Test Module, TTM), blue part (Frame Synchronization Test Module, FSTM), maroon part (Fading Test and Error-Free Test Module, FETM) in Fig. 1. Their details are illustrated in the next subsections. It needs to mention that the Bit Synchronization Module (BSM) is established on the basis of the FPGA gigabit transceiver core. Beyond these modules, the dashed rectangle denotes the Optical Sampling Module (OSM) recording the optical power. Thanks to the log-amplifier after the PIN photodiode, a large dynamic range can be achieved. Due to the fact that coherence time has the magnitude of millisecond, we may choose the analog to digital converter (A/D) with the sampling frequency f_p of several million samples per second. We define $I(k)$ as the k -th received power sample.

It's also found in Fig. 1 that $s_{re}(n)$ represents n -th bit of the baseband input signal after bit synchronization progress. Without loss of generality, the pseudo-random binary sequence (PRBS) is a common choice as the data source. We can benefit a quick synchronization from its sharp autocorrelation function. The n -th bit $s_{loc}(n)$ of error-free PRBS data can also be created by the Local Sequence Module (LSM), which performs as a control group for BER calculation module.

2.1 Synchronization and Outage Measurement

To begin with, the synchronization and outage mechanisms are defined. The sync and loss-sync states are evaluating the packet level, while the bit level synchronization state is determined by the BSM. In this paper, we take the BER as the main judgment criteria for the sync or loss-sync decision. Besides, the received power contributes an auxiliary indication for the loss-sync determination. This will be a wise choice especially for the case of FSO channel with tough ISI, where we may notice the BER is rather unacceptable while the received power is fine.

Fig. 2 shows the switching conditions between sync and loss-sync states. With current loss-sync state, the next state will change into sync state if continuous $N_{e-f,th}$ bits are error free, i.e. satisfying $s_{re}(n) = s_{loc}(n)$. That is to say, the state will remain loss-sync if the number of continuous error-free bits are less smaller than $N_{e-f,th}$, such as the case in the middle of Fig. 2. Note that the values of $N_{e-f,th}$ should be chosen carefully, which will be discussed in the Appendix. Small $N_{e-f,th}$ will lead to avoid state switching frequently, while large $N_{e-f,th}$ wastes more time in determining the states. Due to the original state is loss-sync, the LSM would take $s_{re}(n)$ as the seed source, and try to produce local synchronous sequence. If the subsequent output $s_{loc}(n)$ acts vastly different from $s_{re}(n)$, the LSM will update the seed source in the same way until it meets the sync condition. It's noticed that the initial state should be the sync state during the measurement.

The previous sync state will become the loss-sync state (i.e. outage state) if the group BER result $P_e^{(k,N)}$ exceeds the loss-sync threshold $P_{e,th}$, where $P_e^{(k,N)}$ denotes the BER results of the k -th

TABLE 2
Pseudo-Code in FSTM

1	Initialization: $B_{syn}^{(i)} = 0, F_{syn}^{(i)} = 0, N_{out}^b = 0, N_{out}^f = 0, N_{re} = 0$;
2	for $k = 1: N_{loop}$
3	if $I(i) < I_{th}$
4	Update $N_{out}^b = N_{out}^b + 1$; Set $B_{syn} = 0, F_{syn} = 0$;
5	else Enter the bit level sync state, i.e. $B_{syn}^{(i)} = 1$;
6	end if
7	Calculate $P_e^{(i,N)} = \text{sum}\{s_{re}(n) \neq s_{loc}(n)\} / N, n = (i-1)N + 1, (i-1)N + 2, \dots, iN$;
8	if $F_{syn}^{(i)} = 0$
9	if $[P_e^{(i,N)}, P_e^{(i+1,N)}, \dots, P_e^{(n_e-f-1,N)}] = 0$
10	Set $F_{syn}^{(i)} = 1$;
11	else Update $N_{out}^f = N_{out}^f + 1$; end if
12	else if $F_{syn}^{(i)} = 1 \& P_e^{(i,N)} > P_{e,th}$
13	Set $F_{syn}^{(i)} = 0$, Update $N_{re} = N_{re} + 1$;
14	end if
15	end for
16	Output $P_{out}^{b,ms} = N_{out}^b / N_{loop}, P_{out}^{f,b,ms} = N_{out}^f / (N_{loop} - N_{out}^b), \{F_{syn}^{(i),ms}\}, N_{re}^{ms}$;

group with N bits. If the received power lower is than receiver's sensitivity I_{th} , an outage event will be also declared. This also saves the unnecessary BER calculations. We define two kinds of outage probabilities on the basis of the two criteria. $P_{out}^b = P(I(k) < I_{th})$ is assumed to be the outage probability caused by channel fading. For convenience, P_{sync} is the complementary value of P_{out}^b , representing the synchronization probability. $P_{out}^{f,b} = P(P_e > P_{e,th}, I > I_{th})$ is calculated in order to evaluate the influence by ISI.

For brevity, the pseudo-code form describing the procedure for the FSTM is given in Table 2. The essential variables are explained below. The grouped BER $P_e^{(k,N)}$ has the length $N = N_{pac}^{se} \cdot B_{syn}^{(i)}$ is the indication of the bit level synchronization (1 or sync, and 0 for loss-sync) for the i -th group. Similarly, the $F_{syn}^{(i)}$ denotes the synchronization indication for the packet level. $\lceil \text{plx} - \text{left} - \text{lceil} \bullet \rceil$ denotes the rounded up function. N_{out}^b and N_{out}^f represent the number of packet with loss-sync state in the bit level and packet level, respectively. N_{re} denotes the number of re-synchronization times in the packet level. Overall, the output of FSTM is summarized as $P_{out}^{b,ms}, P_{out}^{f,b,ms}, F_{syn}^{(i),ms}$ and N_{re}^{ms} .

Note that two main parameters $N_{e-f,th}$ and N can determine the probability of false synchronization events and false outage events. Either event can lead to error propagation, which restricts the measurement accuracy. The selection principles of which are given in the Appendix, such that error propagation can be ignored.

2.2 BER and Throughput Analysis

This subsection discusses the calculation progress of BCM and TTM. The BCM compares the two input $s_{re}(n)$ and $s_{loc}(n)$, and records the discrepant bit percent and exports the relevant message to the neighboring modules. After achieving the grouped BER $P_e^{(k,N)}$, the FCT defines $F_{e-f}^{(k)}$ as the sign whether the k -th group is error free $F_{e-f}^{(k)} = 1$ or not $F_{e-f}^{(k)} = 0$. The statistical distribution $f_{P_e}(P_e)$ of grouped BER could also be obtained. It's also mentioned that the group length N can be modified by the Host PC dynamically.

The TTM has the ability of calculating the throughputs in the bit level Θ_b and packet level Θ_{pac} . The above mentioned throughputs are defined as the number of correctly transmitted bits (or packets) per unit time. That is to say, the package is considered as not correctly transmitted even with a single wrong bit. The bit level throughput Θ_b can be calculated by the taking the average of $\Theta_b^{(i)}$, where the superscript i denotes the result for the i -th group. Note that the $\Theta_b^{(i)}$ is equal to 0 when the i -th group has the bit state of loss-sync. The pseudo-code form presenting the procedure for the BCM and TTM is given in Table 3.

2.3 Error-Free and Fading Statistics

The two main features of FSTM are illustrated in this subsection, which are evaluating error-free histograms H_{e-f} and fading histograms H_{fad} , respectively. The error-free mechanism is recapitulated

TABLE 3
Pseudo-Code in BCM and TTM

1	Initialization: $\Theta_b = 0, \Theta_{pac} = 0, \{F_{e-f}^{(k)}\} = 0$;
2	for $i = 1: \lfloor N_{loop}/N \rfloor$
3	Calculate $P_e^{(i,N)} = \text{sum}\{s_{re}(n) = s_{loc}(n)\} / N$,
4	$n = (i-1)N + 1, (i-1)N + 2, \dots, iN$;
5	if $B_{syn} = 1 \& P_e^{(i,N)}$
6	Set $F_{e-f}^{(k)} = 1$;
7	else
8	Set $F_{e-f}^{(k)} = 0$;
9	end if
10	Output $\Theta_b^{(i),ms} = [B_{syn}^{(i)} == 1] ? [1 - \text{mean}\{P_e^{(i,N)}\}] : 0$,
11	$\Theta_{pac}^{ms} = \text{sum}(F_{e-f}^{(k)}) / N_{loop} \cdot N, f_{P_e}^{ms}(P_e) = \text{Histogram } P_e^{(i,N)}$;

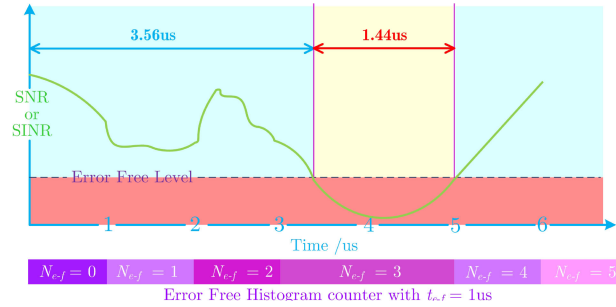


Fig. 3. The diagrammatic sketch of calculating H_{e-f} .

TABLE 4
Pseudo-Code of FSTM Measurement

1	Initialization: $N_{e-f} = 0, N_{fad} = 0, i = 0$;
2	for $i = 1: \lfloor N_{loop}/l_{e-f} \rfloor$
3	if $[F_{e-f}^{(i)}, F_{e-f}^{(i+1)}, \dots, F_{e-f}^{(i+l_{e-f}-1)}] = 0$
4	Update $N_{e-f} = N_{e-f} + 1$;
5	end if
6	end for
7	for $i = 1: \lfloor N_{loop}/l_{fad} \rfloor$
8	if $[F_{syn}^{(i)}, F_{syn}^{(i+1)}, \dots, F_{syn}^{(i+l_{fad}-1)}] = 0$
9	Update $N_{fad} = N_{fad} + 1, i = i + l_{fad}$;
10	end if
11	end for
12	Output $H_{e-f}^{t_{e-f},ms} = N_{e-f} \cdot l_{e-f} / N_{loop}$,
	$H_{fad}^{t_{fad},ms} = N_{fad} \cdot l_{fad} / N_{loop}$,
	$T_{fad}^{mean,ms} = \text{mean}\{H_{fad}^{t_{fad},ms}\}$;

in Fig. 3. Assuming t_{e-f} to be the error-free time to be analyzed, the corresponding error-free group length should be equal to $l_{e-f} = t_{e-f} / (N \cdot T_b)$. For the i -th group with the length of l_{e-f} , the error-free counter N_{e-f} will be increased by one, if all the bits in this group are error-free. As shown in Fig. 3, the first three group has the status of error-free, and N_{e-f} increases continuously until the fourth group. Note that the bits involved calculations start at the beginning of 5us for the sixth group rather than the 4.8us, even the error-free status returns at 4.8us. The histograms of H_{e-f} can be obtained by choosing sufficient numbers of different t_{e-f} . It's also assumed that $H_{e-f}^{t_{e-f}}$ denotes the error-free probability with the group length t_{e-f} .

Similar as the error-free statistics procedure, t_{fad} and N_{fad} are also defined, as well as $l_{fad} = t_{fad} / (N \cdot T_b)$. $H_{fad}^{t_{fad}}$ is also supposed to be the fading probability with the group length t_{fad} . The histograms H_{fad} can be achieved by collecting several measurements with different t_{fad} . In the progress of fading calculation, the mean fading time T_{fad}^{mean} can be also measured. The pseudo-code of FSTM measurement is given in Table 4.

3. Theoretical Analysis

In order to verify the validity of the FCT, this section deduces the theoretical expressions for the measurement results. It will be depicted in Section 4.1 that the indoor experiment results behave consistently as the theoretical results. The analyses in this section have the same order of Section 2, which are outage performance, BER and throughput, fading statistics, respectively. Note that the FCT can be applied in different modulation schemes. This section only focus on the IM/DD circumstance due to the simplicity for experiment implementations.

3.1 Outage Probability

This subsection deduces the outage probability in the IM/DD OWC link without or with the ISI. In the ISI-free case, the received photoelectric signal y out of photo-detector can be modeled in Eq. 1.

$$y = \eta \cdot h \cdot x + n \quad (1)$$

where x represents the data signal choosing from $x \in \{0, 2P_t R_b\}$. h denotes the channel gain. P_t is the mean transmitting power. $R_b = 1/T_b$ stands for the data rate. η denotes the responsivity.

On the basis of Ref. [15], [22], the turbulence channel encompasses the atmospheric turbulence and Rayleigh pointing errors, with the PDF shown in Eq. 2.

$$f_h(h) = \frac{\alpha\beta\rho^2}{A_0 \cdot h_l \Gamma(\alpha) \Gamma(\beta)} G_{1,3}^{3,0} \left(\frac{\alpha\beta h}{A_0 \cdot h_l} \middle| \rho^2 - 1, \alpha - 1, \beta - 1 \right), \quad (2)$$

where $G_{p,q}^{m,n}(x | \mathbf{a}_p = a_1, a_2, \dots, a_p; \mathbf{b}_q = b_1, b_2, \dots, b_q)$ is the Meijer G function. α and β represent the effective numbers of large and small scale turbulent eddies, respectively. $\Gamma(\bullet)$ is the Gamma function. A_0 denotes the maximum fraction of the collected power in the receiving lens. $\rho = w_{zeq} 2\sigma_s$ represents the ratio between the equivalent beam radius w_{zeq} and the displacement standard deviation σ_s .

Seeing that the noise n has a Gaussian distribution with the variance of σ_n^2 and mean value of zero. According to the definition of P_{out}^b , the theoretical expression of $P_{out}^{b,th}$ can be deduced from the integral operation of Eq. 2, shown in Eq. 3.

$$P_{out}^{b,theo} = \frac{\alpha\beta\rho^2}{A_0 \cdot h_l \Gamma(\alpha) \Gamma(\beta)} \cdot \left[\beta \left(\frac{\alpha\beta h_{th}}{h_l \cdot P_t} \right)^\alpha \Gamma(\beta - \alpha) \mathcal{A}(\alpha) + \alpha \left(\frac{\alpha\beta h_{th}}{h_l \cdot P_t} \right)^\beta \Gamma(\alpha - \beta) \mathcal{A}(\beta) + \alpha\beta \Gamma(\alpha - \rho^2) \Gamma(\beta - \rho^2) \left(\frac{\alpha\beta h_{th}}{h_l \cdot P_t} \right)^{\rho^2} - \alpha\beta \Gamma(\alpha) \Gamma(\beta) \right] \quad (3)$$

The function $\mathcal{A}(z)$ is illustrated in Eq. 4, and ${}_1F_2(\bullet)$ stands for the Hypergeometric function.

$$\mathcal{A}(z) = {}_1F_2 \left(z; z + 1, (-1)^{\varpi(z)} (-\alpha + \beta + 1); \frac{\alpha\beta h_{th}}{A_0 \cdot h_l \cdot P_t} \right) + (-1)^{\varpi(z)} \frac{z}{\rho^2 - z} {}_1F_2 \left(z - \rho^2; (-1)^{\varpi(z)} (-\alpha + \beta + 1), z - \rho^2 + 1; \frac{\alpha\beta h_{th}}{A_0 \cdot h_l \cdot P_t} \right), \quad (4)$$

where $\varpi(z)$ is the selection function $\varpi(z) = \begin{cases} 1, & z = \alpha \\ 0, & z = \beta \end{cases}$.

As stated in Section 2, the $P_{out}^{f,b}$ will not be equal to zero, when ISI exists. In accordance with our previous work, the ISI can be brought from timing errors [14], [15]. We consider this scene, where the timing error ξ obeys the Gaussian distribution with zero mean and variance of σ_ξ^2 . The SINR $\tilde{\gamma}$ can be calculated by $\frac{\eta^2 h^2 P_t^2 (1 - |\xi|)}{\sigma_n^2 R_b + |\xi| \eta^2 h^2 P_t^2}$. Assuming that the outage threshold is γ_{th} , we can deduce the

$P_{out}^{f,b,theo}$ leading from ξ .

$$P_{out}^{f,b,theo} = E [P[\tilde{\gamma}, h > I_{th}/P_t]] = \int_{I_{th}/P_t}^{\infty} \frac{\alpha \beta \rho^2}{A_0 \cdot h_l \Gamma(\alpha) \Gamma(\beta)} \operatorname{erf} \left[\frac{1 - \gamma_{th} \sigma_n^2 R_b / \eta^2 h^2 P_t^2}{\sqrt{2} \sigma_\xi (1 + \gamma_{th})} \right] \mathbf{G}_{1,3}^{3,0} \left(\frac{\alpha \beta h}{A_0 \cdot h_l} \right) dh, \quad (5)$$

where $\operatorname{erf}(\bullet)$ denotes the Gauss error function.

By summing the probabilities in Eq. 3 and Eq. 5, the theoretical outage probability can be derived in Eq. 6. Note that the synchronization probability can be easily obtained by the linear operation of $P_{out}^{a,theo}$ and $P_{out}^{b,theo}$. Therefore, the no ink will be wasted here describing the derivation process.

$$\begin{aligned} P_{out}^{theo} &= \frac{\alpha \beta \rho^2}{A_0 \cdot h_l \Gamma(\alpha) \Gamma(\beta)} \left[\int_{I_{th}/P_t}^{\infty} \operatorname{erf} \left[\frac{1 - \gamma_{th} \sigma_n^2 R_b / \eta^2 h^2 P_t^2}{\sqrt{2} \sigma_\xi (1 + \gamma_{th})} \right] \mathbf{G}_{1,3}^{3,0} \left(\frac{\alpha \beta h}{A_0 \cdot h_l} \right) dh \right. \\ &\quad + \beta \left(\frac{\alpha \beta I_{th}}{h_l \cdot P_t} \right)^\alpha \Gamma(\beta - \alpha) A(\alpha) + \alpha \left(\frac{\alpha \beta I_{th}}{h_l \cdot P_t} \right)^\beta \Gamma(\alpha - \beta) A(\beta) \\ &\quad \left. + \alpha \beta \Gamma(\alpha - \rho^2) \Gamma(\beta - \rho^2) \left(\frac{\alpha \beta I_{th}}{h_l \cdot P_t} \right)^{\rho^2} - \alpha \beta \Gamma(\alpha) \Gamma(\beta) \right] \quad (6) \end{aligned}$$

3.2 BER and Distribution

In this subsection, the case with or without ISI are debated. Then the closed form of BER's distribution is also derived under the circumstance of no ISI. Due to the fact that expressions of throughput can be simply deduced from the BER result, the deducing progresses are not mentioned here.

The theoretical expression of BER without ISI is analyzed first. The instantaneous SNR γ can be deduces as $\gamma = \frac{\eta^2 \cdot h^2 \cdot P_t^2}{\sigma_n^2 R_b}$. On the basis of the h 's PDF in Eq. 2, the BER expression $P_{e,isi}^{theo}$ is derived in Eq. 7.

$$\begin{aligned} P_{e,isi}^{theo} &= E \left[Q \left(\sqrt{\gamma/2} \right) \right] = E \left[Q \left(\frac{\eta \cdot h \cdot P_t}{\sigma_n \sqrt{R_b}} \right) \right] \\ &\approx \frac{2^{\alpha+\beta} \eta^2}{96\pi \Gamma(\alpha) \Gamma(\beta)} \left\{ \mathbf{G}_{5,2}^{1,5} \left(\frac{8\eta^2 \bar{P}_t^2 A_0^2}{\alpha^2 \beta^2 R_b \sigma_n^2} \mid \frac{2-\eta^2}{2}, \frac{1-\alpha}{2}, \frac{2-\alpha}{2}, \frac{1-\beta}{2}, \frac{2-\beta}{2}, 0, -\frac{\eta^2}{2} \right) \right. \\ &\quad \left. + 3\mathbf{G}_{5,2}^{1,5} \left(\frac{32\eta^2 \bar{P}_t^2 A_0^2}{3\alpha^2 \beta^2 R_b \sigma_n^2} \mid \frac{2-\eta^2}{2}, \frac{1-\alpha}{2}, \frac{2-\alpha}{2}, \frac{1-\beta}{2}, \frac{2-\beta}{2}, 0, -\frac{\eta^2}{2} \right) \right] \quad (7) \end{aligned}$$

In the case of ISI, the issue of timing error ξ is considered. With the SINR $\tilde{\gamma}$ mentioned above, the expression of BER with ISI is obtained in Eq. 8. During the derivation, the Gaussian-Hermite polynomials are utilized. w_i and x_i denote the roots and the weights of i -th-order Hermite polynomials, respectively. $Q(\bullet)$ represents the Q-function.

$$\begin{aligned} P_{e,isi}^{theo} &= \mathbf{E} \left[Q \left(\sqrt{\tilde{\gamma}/2} \right) \right] = \mathbf{E}_{h,\xi} \left[Q \left(\frac{\eta \cdot h \cdot P_t (1 - \xi)}{\sigma_n \sqrt{R_b} + \xi \eta \cdot h \cdot P_t} \right) \right] \\ &\approx \frac{2^{\alpha+\beta-1} \eta^2}{\sigma_\xi^{1.5} 96\pi^{3/2} \Gamma(\alpha) \Gamma(\beta)} \sum_{i=-10, i \neq 0}^{10} w_i \left\{ \mathbf{G}_{5,2}^{1,5} \left(\frac{8\eta^2 P_t^2 A_0^2 (1 - \sqrt{2} \sigma_\xi x_i)^2}{R_b \alpha^2 \beta^2 \sigma_n^2 + 8\sqrt{2} \sigma_\xi x_i \eta^2 P_t^2 A_0^2} \right) \right. \\ &\quad \left. + 3\mathbf{G}_{5,2}^{1,5} \left(\frac{32R^2 P_t^2 A_0^2 (1 - \sqrt{2} \sigma_\xi x_i)^2}{3R_b \alpha^2 \beta^2 \sigma_n^2 + 32\sqrt{2} \sigma_\xi x_i R^2 \bar{P}_t^2 A_0^2} \right) \right] \quad (8) \end{aligned}$$

The distribution of BER is deduced as follows. It needs to be mentioned that the case of BER with ISI is so complicated to get the closed-form PDF. Therefore, we discuss the distribution of BER without ISI. We will start with the Cumulative Distribution Function (CDF) $F_p(p)$. Noting the

difficulty in deriving the inverse function of the Q-function, we use the approximation instead, which is $Q(x) = \frac{1}{2} - \frac{1}{2} \tanh(\mu x + v x^3)$. μ and v can be considered as constant values. Thus the inverse function is deduced as $Q^{-1}(x) \approx \tau \sinh[\frac{1}{3} \sinh^{-1}(v \cdot \tanh^{-1}(1 - 2x))]$, where τ and v are deduced from μ and v , i.e. $\tau = 2(\mu/3v)^{1/2}$, $v = 1/2v(\mu/3v)^{-3/2}$. Therefore, the CDF $F_P(p)$ is derived in Eq. 9.

$$F_P(p) = P[P_e < p] \approx P\left[h > Q^{-1}\left(\frac{\sigma_n \sqrt{R_b}}{\eta \cdot P_t} p\right)\right] \\ \approx 1 - F_h\left[\tau \sinh\left[\frac{1}{3} \sinh^{-1}\left(v \cdot \tanh^{-1}\left(1 - 2\frac{\sigma_n \sqrt{R_b}}{\eta \cdot P_t} p\right)\right)\right]\right], \quad (9)$$

where $F_h(h)$ denotes the CDF of h .

The PDF of BER can be obtained by taking the derivation of Eq. 9, which is

$$f_{P_e}^{theo}(P_e) = \frac{d}{dp} \left\{ 1 - F_h\left[\tau \sinh\left[\frac{1}{3} \sinh^{-1}\left(v \cdot \tanh^{-1}\left(1 - 2\frac{\sigma_n \sqrt{R_b}}{\eta \cdot P_t} p\right)\right)\right]\right]\right\} \\ = \frac{\alpha \beta \eta P_t \rho^2}{A_0 \cdot h_l \Gamma(\alpha) \Gamma(\beta) \sigma_n \sqrt{R_b}} \cdot \exp\left(-\frac{\sigma_n^2 R_b P_e^2}{2 \eta^2 P_t^2}\right)^{-1} \\ \cdot \mathbf{G}_{1,3}^{3,0}\left(\frac{\alpha \beta}{A_0 \cdot h_l} \tau \sinh\left[\frac{1}{3} \sinh^{-1}\left(v \cdot \tanh^{-1}\left(1 - 2\frac{\sigma_n \sqrt{R_b}}{\eta \cdot P_t} P_e\right)\right)\right]\right). \quad (10)$$

3.3 Mean Fading Time

The derivation of mean fading time is depicted in this subsection. The mean fading time can be calculated by the expected number of fades per unit time $N_{h_{th}}^{theo}$ and outage probability P_{out} . $N_{h_{th}}^{theo}$ is defined as the number of negative (or positive) crossings of a prescribed threshold h_{th} . In order to derive $N_{h_{th}}^{theo}$, the joint PDF of the channel gain h and its time derivative h' is defined in Eq. 11.

$$f_{h,h'}(h, h') \cong f_h(h) \cdot f_{h'}(h'|h) \quad (11)$$

According to Ref. [23], the conditional PDF $f_{h'}(h'|h)$ can be modeled as Gaussian distribution.

$$f_{h'}(h'|h) = \frac{1}{2\sqrt{2\pi} \varepsilon_0 \sigma_h} \exp\left(-\frac{h'^2}{8\pi^2 \varepsilon_0^2 \sigma_h^2 h}\right), \quad (12)$$

where ε_0 denotes the quasi-frequency. σ_h^2 is the variance of h .

By assuming $h_{th} = l_{th}/P_t$, $N_{h_{th}}^{theo}$ can be derived in Eq. 13.

$$N_{h_{th}}^{theo} = \frac{1}{2} \int_{-\infty}^{\infty} |h'| \cdot f_{h,h'}(l_{th} P_t, h') dh' = \frac{\sqrt{2\pi} \alpha \beta \rho^2 \varepsilon_0 \sigma_h}{A_0 \cdot h_l \Gamma(\alpha) \Gamma(\beta)} \mathbf{G}_{1,3}^{3,0}\left(\frac{\alpha \beta l_{th}}{A_0 \cdot h_l \cdot P_t} \middle| \rho^2 - 1, \alpha - 1, \beta - 1\right) \rho^2 \quad (13)$$

Therefore the mean fading time $T_{fad}^{mean,theo}$ is deduced, given in Eq. 14, which can be considered as a function of h_{th} . For the ISI free case, the integral term can be abandoned.

$$T_{fad}^{mean,theo} = \frac{1}{\sqrt{2\pi} \varepsilon_0 \sigma_h} \mathbf{G}_{1,3}^{3,0}\left(\frac{\alpha \beta l_{th}}{A_0 \cdot h_l \cdot P_t} \middle| \rho^2 - 1, \alpha - 1, \beta - 1\right)^{-1} \\ \cdot \left[\int_{l_{th}/P_t}^{\infty} \operatorname{erf}\left[\frac{1 - \gamma_{th} \sigma_n^2 R_b / \eta^2 h^2 P_t^2}{\sqrt{2} \sigma_\xi (1 + \gamma_{th})}\right] \mathbf{G}_{1,3}^{3,0}\left(\frac{\alpha \beta h}{A_0 \cdot h_l}\right) dh \right. \\ \left. + \beta \left(\frac{\alpha \beta l_{th}}{h_l \cdot P_t}\right)^\alpha \Gamma(\beta - \alpha) A(\alpha) + \alpha \left(\frac{\alpha \beta l_{th}}{h_l \cdot P_t}\right)^\beta \Gamma(\alpha - \beta) A(\beta) \right. \\ \left. + \alpha \beta \Gamma(\alpha - \rho^2) \Gamma(\beta - \rho^2) \left(\frac{\alpha \beta l_{th}}{h_l \cdot P_t}\right)^{\rho^2} - \alpha \beta \Gamma(\alpha) \Gamma(\beta) \right] \quad (14)$$

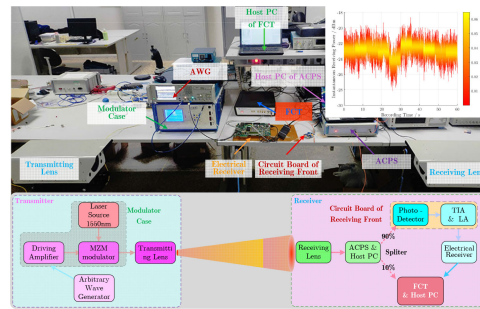


Fig. 4. The block diagram and the scene of the indoor experiment.

4. Experiment Performance

In this section, two experiments are illustrated. The purpose of the first indoor experiment is to verify the validity of the FCT. It will be found that the experimental results behave virtually identically as the theoretical expressions deduced in Section 3. Another field experiment is finished, and the results of FCT are also reported.

4.1 The Indoor Verification Experiment

In the indoor experiment, the arbitrary wave generator (AWG, Tektronix AWG70002 A) is the data source producing the PRBS sequence, where ISI can be chosen optionally. The data rate is set to be 10 Gbps. After modulated by the Mach-Zehnder modulator (MZM), optical modulation signal enters the space, with the help of the transmitting lens. The receiver couples the collected signal into a multimode fiber. The turbulence channel is simulated by the atmosphere scintillation playback system (ACPS), where the data of channel gain would be transmitted from another host computer by the Ethernet interface. It can attenuate the input optical signal dynamically ranging from 0 dB to 30 dB, with the minimum time resolution of 1 μ s. Either the input or output interface of the ACPS is multi-mode FC/PC fiber. The northeast side of Fig. 4 shows the received power. The pseudo-color bar indicates that the channel gain are consistent with the theoretical distribution in Eq. 2. During the indoor environment, we simulate the turbulence channel with $\alpha = 2$, $\beta = 1$ for strong turbulence, and $\alpha = 4$, $\beta = 2$ for weak turbulence. The fading channels caused by pointing errors are simulated with the parameters of $A_0 = \text{erf}(\frac{\sqrt{\pi/2}}{10}) = 0.0198$, $w_{zeq} = 2.0105$, $\sigma_s = 0.2$ (i.e. $\rho = 5.0263$). The theoretical variance of normalized optical power is equal to $\frac{1+\rho^2}{\rho^2}(\alpha^{-1} + \beta^{-1} + \alpha^{-1}\beta^{-1} + \frac{1}{1+\rho^2}) = 0.9492(\alpha = 4, \beta = 2)$ or $2.1187(\alpha = 2, \beta = 1)$, while the collected power fluctuation is equal to $0.9495(\alpha = 4, \beta = 2)$ or $2.1193(\alpha = 2, \beta = 1)$, which ensures that the experimental results are consistent with the theoretical values in Fig. 5 and Fig. 6. The optical receiver exports the baseband signal to the FCT. An optical splitter is used to provide 10 percent of the received optical power to the FCT.

The performance of outage probability, BER and mean fading time are arrayed in Fig. 5(a)–5(c), respectively, which has the same order as Section 3. These three figures have one thing in common that the theoretical results are almost exactly consistent with the experimental ones, which describes the measurement accuracy. It could be found from Fig. 5(a) that the outage probability P_{out} is larger than P_{out}^b in the case of ISI. Large ISI can degrade the performance seriously, which explained again the necessity of combining BER and received power as the outage criteria rather than only using power or only using BER.

The instantaneous BER is furnished in Fig. 6(a), while the Fig. 6(b) furnishes the distribution of BER. Fig. 6(a) shows that the worse BER has larger probabilities, which is caused by the distribution of h . There are also two intervals where BER are not calculated. It's because the two intervals have the packet states of loss-sync. It's mentioned that Fig. 6(b) only listed

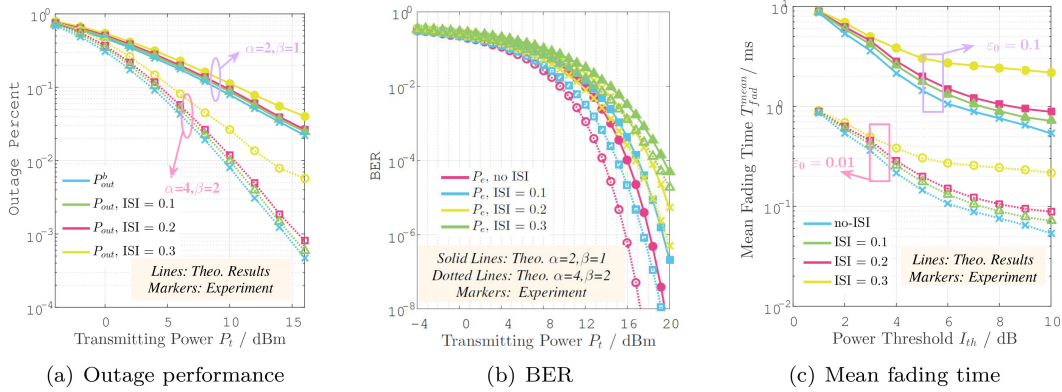


Fig. 5. Indoor experimental results versus theoretical ones.

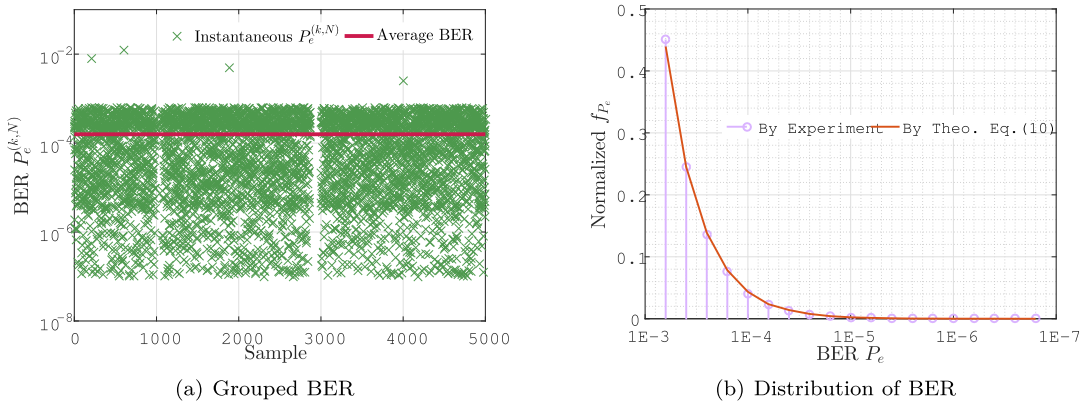


Fig. 6. Grouped BER and its distribution.

the histogram with BER ranging from 10^{-7} to 10^{-3} . And the theoretical distribution in Eq. 10 needs to be normalized by the sum of the probabilities in this range.

4.2 The Field Measurement Experiment

An OWC experiment of 1.9 km is illustrated in this subsection. Then relevant results are revealed, where the algorithms stated in Section 2 are employed. Fig. 7 integrates the scene of transmitting end and receiving end, as well as their locations. The wavelength is chosen as 1550 nm. The ambient temperature changed from -3°C to 8°C . The wind during the experiment came from southwestern direction with the wind speed ranging from light air to moderate breeze (i.e. 0.1 m/s to 7.5 m/s). The variance of collected optical power ranged from 0.37 to 2.52, which indicated the turbulence covered weak and strong conditions. We choose PRBS10 as the data source with the rate of 2.5 Gbps, whose feedback polynomial is $x^{10} + x^7 + 1 = 0$. For tracking the received beam, a fast steering mirror (FSM) is utilized at the receiver according to the output of the quadrant detector (QD). The input of QD is part of the received beam with the split ratio of 1%. The values of $P_{e,th}^{se}$, I_{th}^{se} , N_{e-f}^{se} are set to be 10^{-3} , -33 dBm, $1E4$, respectively.

Fig. 8(a) depicts the outage probabilities where the outage criteria is combining P_e and $I(k)$. The outage performance is also listed as a control group triggered by $I(k)$. The vertical discrepancy of the markers with the same transmitting power reveals the outage crippled by ISI, i.e. $P_{out}^{f,b}$. It proves

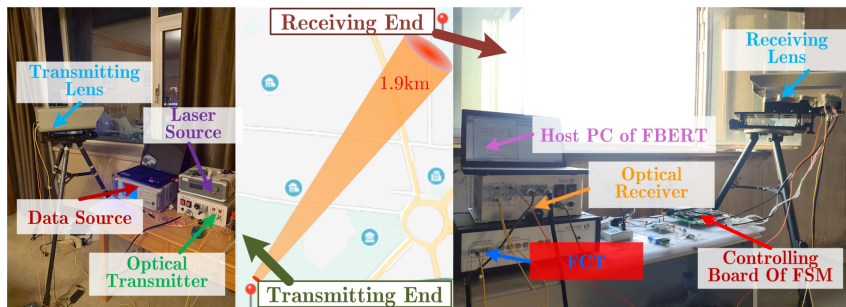
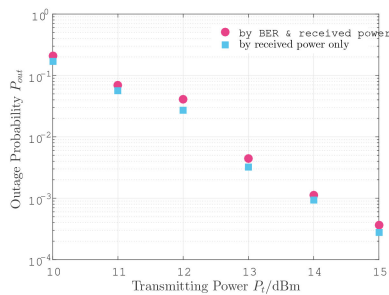
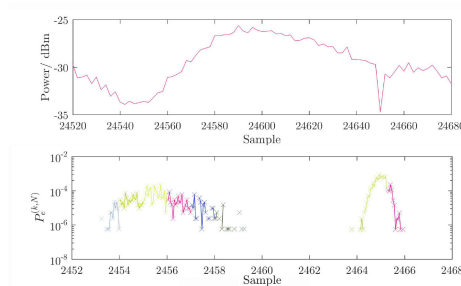


Fig. 7. The scenes of the transmitting end and receiving end for the 1.9 km field trial link.

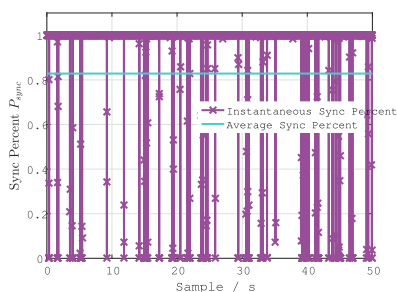


(a) Outage probability

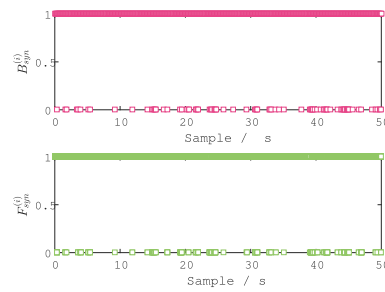


(b) Optical power versus grouped BER

Fig. 8. Outage Performance.



(a) Sync probability



(b) Sync status

Fig. 9. Synchronization performance in bit and packet level.

the need of recording received power and the BER simultaneously. A period of 16 ms instantaneous sample of BER and received power are compared in Fig. 8(b). It could be found that the BER and received power are in correspondence with each other in the time domain.

Fig. 9(a) illustrates the synchronization percent P_{sync}^{ms} , while Fig. 9(b) reveals the corresponding status in the bit and packet level. With the transmitting power to be 0 dBm, the average sync percent P_{sync}^{ms} is 82.6%. The fading events have occurred for 62 times with the duration of 50 seconds. Besides, it could be obtained from Fig. 9(b) that $F_{syn}^{(i),ms}$ ought to be zero when the corresponding $B_{syn}^{(i),ms}$ is zero, but it's not necessarily in the contrary case. It can be explained in this way that the received power lower than I_{th} will bring about the loss-sync states occurring in the bit level, also

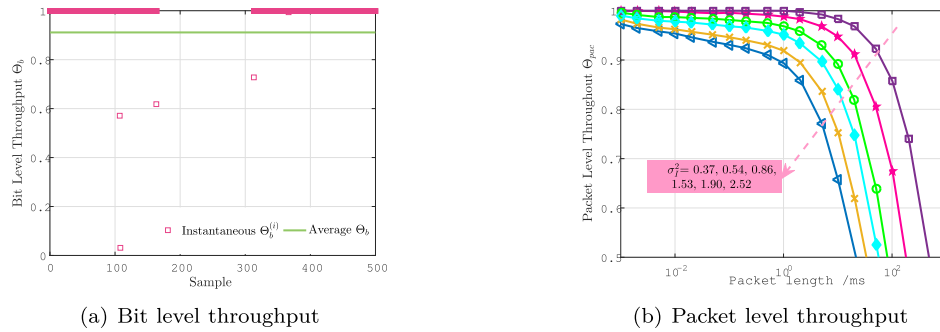


Fig. 10. Throughput results by field trial.

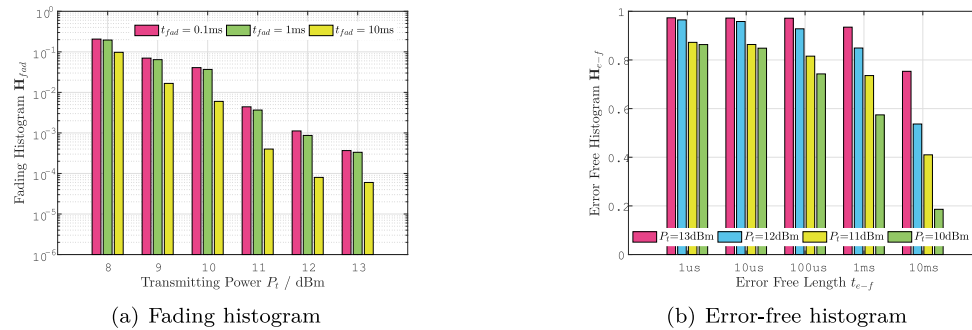


Fig. 11. Histogram results by field trial.

in the packet level. The loss-sync states caused by ISI in the packet level even when the received power exceeds the sensitivity.

Fig. 10(a) and Fig. 10(b) reveal the throughput in the bit level and the packet level, respectively. It can be seen from Fig. 10(a) that the average throughput Θ_b^{ms} is $0.919 \times 2.5 = 2.2975$ Gbps. That is to say, the maximum available rate is 2.2976 Gbps. The data with larger rates cannot achieve a correct transmission. As a whole, there are three outage events which are the 107-th sample, 108-th sample, and the period between the 169-th sample and the 312-th sample. Both of the first two outage events are less than 0.1 ms. The third outage event has a fading interval of 14.3 ms. Different packet throughput Θ_{pac}^{ms} are listed with various packet lengths. The experiments with kinds of variances of the received power are measured in different weather. It can be revealed from Fig. 10(b) that the packet length is suggested to be smaller than 1 ms in order to achieve throughput larger than 0.9.

The fading histograms H_{fad} and error-free histograms H_{e-f} are illustrated in Fig. 11(a) and Fig. 11(b), respectively. According to Fig. 11(a), most fading events have the time smaller than 10 ms. What's more, no fading exceeds 100 ms, where the longest fading time is 24.3 ms. The mean fading time is 2.7 ms, while the mean time between fades is 67.8 ms. These fading data can provide evidences for the channel for design the mitigation of the fluctuations, such as suitable interleaving depth or suited packet length in ARQ scheme. With this method, the redundant processing time can be saved, as well as the hardware resources. It can be also obtained that probability of fading with the length of 10 ms always maintains larger than 0.1% even with sufficient transmitting power. By comparing Fig. 11(a) and Fig. 11(b) with the transmitting power of 10 dBm, the fading probability of 0.1 ms is almost complementary to the error-free probabilities smaller than 0.1 ms. That is to say, the coherence time has the magnitude of 0.1 ms, which is verified by the optical power results that the coherence time is 0.17 ms. The optimal packet length should have the similar magnitude.

5. Conclusion

In this manuscript, we have proposed and demonstrated the principle of a FCT, as well as the implementation based on FPGA. The FCT has the ability of obtaining the outage and synchronization probability, where both the BER and received optical power are considered as the threshold. In this way, the degradation brought by ISI can be evaluated. The BER and throughput are also derived in the bit level and the packet level. Besides, the error-free and fading statistics can be obtained. In order to verify the effectiveness, we carry out the indoor experiments, whose results are virtually identical with the theoretical expressions of outage probability, BER and its distribution, mean fading time. Then a field trial of 1.9 km has been conducted to character the fading channel, where corresponding results and analyses are illustrated. The main purpose of the designed FCT is not only to evaluate the link objectively and comprehensively, but to improve the system's performance according to the measurements, such as designing optimal packet based network protocols, formulating the efficient FEC or ARQ schemes, setting suitable interleaving depth.

Appendix

As illustrated before, our main switching strategy of sync-in and sync-out is comparing the packet bit error rate $P_e^{(k,N)}$ and the threshold $P_{e,th}$. If the false synchronization event happens, the error propagation will lead to make the BER measurement inaccurate. For the PRBS sequence created by L -order registers, the sharp autocorrelation function has only two values, which are 1 and $1/(2^L - 1)$, respectively. Thus it's almost impossible that false synchronization events happen caused by incorrectly aligning the sequence. As a result, we need only consider the case that continuous N bit are error free but the mean BER P_e is worse than the threshold $P_{e,th}$. The number of error bits N_{err} in a packet length of $N_{e-f,th}$ bits follows the Poisson distribution, given in Eq. A1.

$$P(N_{err}) = N_{e-f,th} \cdot P_e \frac{\exp(-N_{e-f,th} \cdot P_e)}{\Gamma(N_{err} + 1)} \quad (A1)$$

Thus the probability of $N_{err} = 0$ can be derived as $P(N_{err} = 0) = \cdot P_e \cdot \exp(-N_{e-f,th} \cdot P_e)$. We need to choose $N_{e-f,th}$ large enough to make sure the $P(N_{err} = 0)$ is sufficient closed to 0, when P_e is worse than $P_{e,th}$. Consider the derivative function given in Eq. (A2), $N_{e-f,th}$ larger than $1/P_{e,th}$ makes $P(N_{err} = 0)$ become a monotonically decreasing function. In this sequel, for any arbitrary current P_e larger than $P_{e,th}$, the event that continuous $N_{e-f,th}$ bits has error free status can have a smaller probability than the situation of $P_e = P_{e,th}$. As a result, we may choose $N_{e-f,th}$ larger than $1/P_{e,th}$ to achieve a more convincing result, which also prevents the synchronization state switching frequently.

$$\frac{d}{dP_e} P(N_{err} = 0) = N_{e-f,th} (1 - N_{e-f,th} \cdot P_e) \cdot \exp(-N \cdot P_e) \quad (A2)$$

In terms of the false outage event, N has to be large enough for the packet BER $P_e^{(k,N)}$ close enough to the actual BER P_e , though the packet BER $P_e^{(k,N)}$ is the unbiased estimation on the actual BER P_e . Herein we introduce δ as the confidence level denoting the probability of actual BER P_e smaller than the $P_{e,th}$. By adopting the binomial theorem, Eq. A3 gives us a hint about the chosen of N .

$$N = \frac{1}{P_{e,th}} \left[-\ln(1 - \delta) + \ln \left(\sum_{k=0}^{N_e} \frac{(N \cdot P_{e,th})^k}{\Gamma(k + 1)} \right) \right] \quad (A3)$$

where N_e denotes the error number in the N bits. For calculation convenience of N , we can ignore the second item in Eq. A3. For example, at least $N = 4605$ bits need to be measured in order to have a 99.000% confidence level for the BER threshold $P_{e,th} = 10^{-3}$.

References

- [1] X. Liu *et al.*, "ABER performance of LDPC-coded OFDM free-space optical communication system over exponentiated weibull fading channels with pointing errors," *IEEE Photon. J.*, vol. 9, no. 4, Aug. 2017, Art. no. 7905113.
- [2] A. Al-Kinani *et al.*, "Optical wireless communication channel measurements and models," *IEEE Commun. Surveys. Tuts.*, vol. 20, no. 3, pp. 1939–1962, Jul.-Sep. 2018.
- [3] H. L. Zhou *et al.*, "Orbital angular momentum complex spectrum analyzer for vortex light based on the rotational Doppler effect," *Light Sci. Appl.*, vol. 6, no. 16251, pp. 1–8, 2016.
- [4] S. Ding, J. Zhang and A. Dang, "Adaptive threshold decision for on-off keying transmission systems in atmospheric turbulence," *Opt. Exp.*, vol. 25, no. 20, pp. 24425–24436, 2017.
- [5] L. Wu, Z. Zhang, and H. Liu, "Modulation scheme based on precoder matrix for MIMO optical wireless communication systems," *IEEE Commun. Lett.*, vol. 16, no. 9, pp. 1516–1519, Sep. 2012.
- [6] M. Niu, J. Cheng and J. F. Holzman, "Alamouti-type STBC for atmospheric optical communication using coherent detection," *IEEE Photon. J.*, vol. 6, no. 1, Feb. 2014, Art. no. 7900217.
- [7] H. Chen *et al.*, "Phase uniformly distributed circular MQAM combined with probabilistic shaping for PM-CO-OFDM systems in satellite-to-ground optical communications," *IEEE Photon. J.*, vol. 11, no. 6, Dec. 2019, Art. no. 7907110.
- [8] Z. Sodnik *et al.*, "LLCD operations using the lunar lasercom OGS terminal," in *Proc. SPIE*, vol. 8971, no. 1, 2014, pp. 1–13.
- [9] E. A. Park, D. Cornwell, and D. Israel, "NASA's next generation ≥ 100 Gbps optical communications relay," in *Proc. IEEE Aerosp. Conf.*, 2019, pp. 1–9.
- [10] L. Yu, B. Hu and Y. Zhang, "Intensity of vortex modes carried by Lommel beam in weak-to-strong non-Kolmogorov turbulence," *Opt. Exp.*, vol. 25, no. 16, pp. 19538–19547, 2017.
- [11] H. G. Olanrewaju and W. O. Popoola, "Effect of Synchronization Error on Optical spatial modulation," *IEEE Trans. Commun.*, vol. 65, no. 12, pp. 5362–5374, Dec. 2017.
- [12] S. Hranilovic, *Wireless Optical Communication Systems*, Springer Science Business Media, 2005.
- [13] Dabiri *et al.*, "Blind signal detection under synchronization errors for FSO links with high mobility," *IEEE Trans. Commun.*, vol. 67, no. 10, pp. 7006–7015, Oct. 2019.
- [14] Y. Li *et al.*, "Timing jitter's influence on the symbol error rate performance of the L -ary pulse position modulation free-space optical link in atmospheric turbulent channels with pointing errors," *Opt. Eng.*, vol. 56, no. 3, pp. 036116, 2017.
- [15] Y. Li *et al.*, "Evaluation on the capacity and outage performance of the free space optical system impaired by timing jitters over an aggregate channel," *Opt. Eng.*, vol. 56, no. 7, pp. 076108, 2017.
- [16] Y. Fan and Z. Zilic, "BER testing of communication interfaces," *IEEE Trans. Instrum. Meas.*, vol. 57, no. 5, pp. 897–906, May 2008.
- [17] A. Xiang *et al.*, "Design and verification of an FPGA-based bit error rate tester," *Phys. Procedia*, vol. 37, no. 1, pp. 1667–1673, 2012.
- [18] G. Vandersteen *et al.*, "Quasi-analytical bit-error-rate analysis technique using best linear approximation modeling," *IEEE Trans. Instrum. Meas.*, vol. 58, no. 2, pp. 475–482, Feb. 2009.
- [19] B. A. Mazzeo and M. Rice, "Bit error rate comparison statistics and hypothesis tests for inverse sampling negative binomial experiments," *IEEE Trans. Commun.*, vol. 64, no. 5, pp. 2192–2203, May 2016.
- [20] M. Kubicek, H. Henniger, and Z. Kolka, "Bit error distribution measurements in the atmospheric optical fading channel," in *Proc. SPIE*, 2008, vol. 6877, pp. 1–8.
- [21] J. E. Sluz *et al.*, "Characterization of data transmission through a maritime free-space optical channel with a custom bit error rate tester," in *Proc. SPIE*, 2010, vol. 7700, pp. 1–11.
- [22] M. R. Bhatnagar and Z. Ghassemlooy, "Performance analysis of gamma-Gamma fading FSO MIMO links with pointing errors," *OSA/IEEE J. Lightw. Technol.*, vol. 34, no. 9, pp. 2158–2169, 2016.
- [23] L. C. Andrews and R. L. Phillips, *Laser Beam Propagation Through Random Media*, 2nd ed., SPIE, 2005.